RSC Advances

PAPER

View Article Online
View Journal | View Issue

Cite this: *RSC Adv.*, 2015, **5**, 32520

Iron-based metal organic framework, MIL-88A, as a heterogeneous persulfate catalyst for decolorization of Rhodamine B in water†

Kun-Yi Andrew Lin,* Hsuan-Ang Chang and Chung-Jun Hsu

While Metal Organic Frameworks (MOFs) have been extensively investigated as photocatalysts to eliminate toxic pollutants in water, studies using MOFs as chemical oxidative catalysts to degrade contaminants are still limited. MOFs used as catalysts for chemical oxidation reactions were prepared in *N*,*N*-dimethylformamide (DMF), a potential carcinogenic solvent. If such MOFs are not well activated and have not properly undergone solvent exchange, DMF can still be encapsulated inside MOFs, leading to secondary pollution. Considering the essence of wastewater treatment and pollutant reduction, DMF-free MOFs which still exhibit the catalytic activity to activate oxidants should be developed. Thus, we selected an iron-based MOF, MIL-88A, which can be prepared using Fe^{3+} with fumaric acid just in water. The as-synthesized MIL-88A is evaluated as the heterogeneous catalyst to activate persulfate for the decolorization of Rhodamine B (RB) dye. Iron oxide clusters (*i.e.*, Fe_2O_3) form within MIL-88A through the coordination of Fe^{3+} and fumaric acid. Fe^{3+} of Fe_2O_3 is expected to induce the generation of persulfate radicals which in turn lead to the formation of sulfate radicals to decolorize RB dye. Factors influencing the activation of persulfate and RB decolorization were examined including persulfate dosage, MIL-88A loading, temperature, pH, UV and US irradiation as well as inhibitors. MIL-88A was assessed for the multiple-cycle activation of persulfate without additional regeneration of spent MIL-88A. These features make MIL-88A an effective and recyclable heterogeneous catalyst for the activation of persulfate.

Received 24th January 2015
Accepted 25th March 2015

DOI: 10.1039/c5ra01447f

www.rsc.org/advances

1. Introduction

Metal Organic Frameworks (MOFs) are intriguing materials that have attracted great attention from both academia and industry. MOFs, consisting of a metal ion as the "node" and ligands as the "bridges", can be designed and synthesized using various species of metals and organics. Thus, MOFs exhibit versatile physical and chemical properties such as controllable pore volume, high surface area, multiple functionalities, high chemical resistance, *etc.*[1–3] Because of these promising characteristics, MOFs have been intensively investigated for gas adsorption/storage,[4–7] catalysis,[8–10] biomedicine,[7,11] photoluminescence,[12] and analytical chemistry.[13]

As the development of MOFs for the above-mentioned areas continues to advance, researchers have begun to investigate the feasibility of using MOFs in aqueous applications. Several MOFs are also found to be stable in aqueous solutions and some are even thought to remain intact under rigorous conditions such as high-temperature and highly basic solutions.[14] Therefore, a number of MOFs have been proposed and evaluated as stationary phase of liquid chromatography,[15–17] adsorbents,[18,19] catalysts,[20,21] *etc.* In particular, MOFs have been used to remove toxic compounds from water *via* adsorption, including halogens,[22] heavy metals,[23] toxic dyes,[24] herbicides,[25] oils,[26] phenols,[27] pharmaceuticals,[28] and humic acid.[29]

Since some MOFs are composed of transition metals and oxygen-containing ligands, the coordination of the transition metals with the oxygen of the ligands creates metal-oxide clusters within the MOFs,[30–32] which can exhibit photo-catalytic activity.[20,21] These photocatalytic MOFs include MOF-5 (Zn–O),[33,34] MIL-series (Fe–O, Cr–O and Ti–O)[32,35,36] and UiO-series (Zr–O).[37–39] A few photocatalytic MOFs have been evaluated for their photocatalytic activity to degrade organic pollutants (*e.g.*, dyes)[32] and to reduce toxic metal ions (*e.g.*, Cr^{6+})[38] in water. However, the MOFs' transition metal–oxygen clusters not only exhibit photocatalytic activity but also biomimetic and chemical catalytic activities.[20,21] In particular, iron-oxide, cobalt-oxide and manganese oxide clusters have been shown to possess superior chemical catalytic activity to activate oxidants (*e.g.*, hydrogen peroxide) in wet chemical oxidation.[40–43] Therefore, MOFs containing iron, cobalt and manganese oxides can be alternative heterogeneous catalysts to activate these oxidants for the degradation of pollutants. A few studies have looked at the feasibility of using MOFs as heterogeneous catalysts for the

Department of Environmental Engineering, National Chung Hsing University, 250 Kuo-Kuang Road, Taichung, Taiwan, Republic of China. E-mail: linky@nchu.edu.tw; Tel: +86-4-22854709

† Electronic supplementary information (ESI) available. See DOI: 10.1039/c5ra01447f

activation of oxidants. Du *et al.* and Ai *et al.* both evaluated MIL-53, an iron-based MOF, as a catalyst for the conventional and photo Fenton reactions to degrade dyes.[44,45] Bhattacharjee *et al.* also used Fe-MOF-74, another iron-based MOF, as the Fenton reaction catalyst to degrade phenol.[46] Another widely investigated iron-based MOF, MIL-101, was also adopted as the catalyst in the photo-Fenton reaction.[47] While these iron-containing MOFs have been shown to activate hydrogen peroxide in the Fenton-based reactions, only one study tested the photocatalytic activity of the iron-containing MOFs to activate another important oxidant, persulfate.[44] However, the emphasis of that study was placed on photocatalytic activity of the iron-based MOFs to generate electrons which can clearly induce the decomposition of persulfate, instead of the conventional persulfate activation.[40–42,48,49] Most importantly, all of the above-mentioned iron-containing MOFs (*i.e.*, MOF-53, Fe-MOF-74, and MIL-101) for the activation of oxidants are prepared in *N*,*N*-dimethylformamide (DMF), a carcinogenic solvent according to the International Agency for Research on Cancer. If MOFs are not well activated and have not properly undergone solvent exchange, DMF can still be encapsulated inside MOFs, leading to secondary pollution. Considering the concerns involved with DMF, minimizing usage of DMF can lower healthy threat during the synthesis and subsequent waste-treatment cost. Avoiding usage of DMF is also expected to shorten the synthesis time by reducing activation and solvent-exchange times. Therefore, DMF-free MOFs that still contain iron oxides should be developed and adopted in such oxidant-activation reactions. In this study, we select an iron-based MOF, MIL-88A, which can be prepared using Fe^{3+} with fumaric acid just in water.[11,50] The as-synthesized MIL-88A is evaluated as the heterogeneous catalyst to activate persulfate for the decolorization of Rhodamine B (RB) dye, as a representative organic pollutant. MIL-88A is also characterized by scanning electronic microscopy (SEM), transmission electronic microscopy (TEM), X-ray diffraction (XRD), FT-IR spectroscopy, X-photoelectron spectroscopy (XPS) as well as thermogravimetric (TG) analysis. To obtain an optimal ratio of RB/persulfate/MIL-88A for the RB degradation, the effects of MIL-88A loading and persulfate dosage were investigated. Effects of temperature, pH, UV irradiation as well as ultrasonication were also examined. A recyclability test was conducted to evaluate the long-term use of MIL-88A to activate persulfate. Given the composition of MIL-88A, a potential mechanism of persulfate activation was also proposed and illustrated schematically.

2. Experimental

2.1 Materials

All chemicals involved in this study are commercially available and used without additional purification. Iron chloride ($FeCl_3 \cdot H_2O$) and ascorbic acid were purchased from Merck (Germany). Fumaric acid, Rhodamine B (RB), methanol, *tert*-butyl alcohol (TBA), sodium persulfate and terephthalic acid were obtained from Sigma-Aldrich (USA). Deionized (D.I.) water was prepared to exhibit less than 18 MOhm cm.

2.2 Preparation of MIL-88A

The preparation of MIL-88A can be illustrated in Fig. 1 according to the reported procedure[11,50] with modifications. Briefly, 0.5 g of $FeCl_3 \cdot H_2O$ and 5 g of fumaric acid were added to 50 ml of D.I. water in a media bottle and the resulting mixture was stirred for 1 hour to fully dissolve these two reagents in D.I. water. Subsequently, the homogeneous solution was capped in the bottle and heated in a conventional oven at 85 °C for 24 hours. The product was collected *via* centrifugation, washed thoroughly with water and ethanol, and dried at 100 °C under reduced pressure. Although other MIL-88 MOFs (*i.e.*, MIL-88B, MIL-88C and MIL-88D) have to be prepared in DMF,[51] we still prepared one of MIL-88 MOFs to evaluate whether other MIL-88 MOFs were also able to activate persulfate. Since MIL-88B, MIL-88C and MIL-88D all consist of dicarboxylic ligands with different numbers of benzene rings (*i.e.*, terephthalic acid, 2,6-naphthalenedicarboxylate, 4,4′-biphenyldicarboxylate, respectively), MIL-88B was particularly selected considering that it is much more structurally similar to MIL-88A. MIL-88B was prepared using $FeCl_3$ with terephthalic acid in DMF according to the reported procedures.[51,52]

2.3 Characterization of MIL-88A

The morphology of MIL-88A was first analyzed using a Field Emission SEM (JEOL JSM-6700, Japan) and Transmission Electronic Microscopy (TEM) (JEOL JEM-2010, Japan). The powder X-ray diffraction (XRD) pattern of MIL-88A was obtained using an X-ray diffractometer (PANalytical, the Netherlands) with copper as an anode material (40 mA, 45 kV). Absorption infrared (IR) spectrum of MIL-88A was measured by a Fourier-Transform Infrared spectrometer (Horiba FT-730, Japan) with KBr pellets as sample holders. The chemical composition of MIL-88A was analyzed using a X-ray Photoelectron Spectroscopy (XPS) (PHI 5000 Versa Probe/Scanning ESCA Microprobe, ULVAC-PHI, Inc., Japan) with a monochromatized Mg Kα (1253.6 eV) X-ray source. Thermogravimetric (TG) curve of MIL-88A was measured using a thermogravimetric analyzer (ISI TGA i1000, USA) at a heating rate of 10 °C min^{-1} from 25 to 800 °C in nitrogen.

2.4 Decolorization of RB using persulfate activated by MIL-88A

Rhodamine B (RB) decolorization using persulfate was evaluated by batch-type experiments. Since MIL-88A can also exhibit

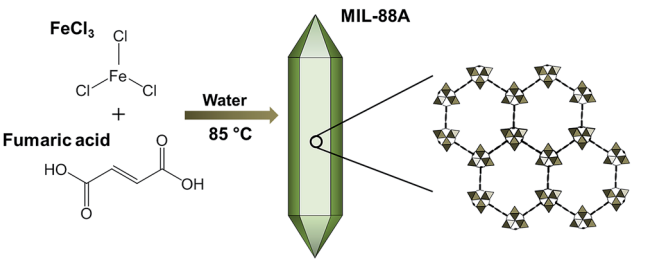

Fig. 1 Schematic illustration of synthesis of MIL-88A.

photocatalytic activity under light irradiation to generate electrons to induce the activation of persulfate, the RB decolorization experiments were all conducted in a dark room. In a typical experiment, 0.05 g of persulfate was added to a 500 ml of RB solution with an initial concentration (C_0) of 10 mg L^{-1}. Prior to adding persulfate, MIL-88A was added to RB solutions and the resulting suspension had to be stirred for 30 min to ensure the adsorption equilibrium between MIL-88A and RB. A given amount of persulfate was subsequently added to the solution to decolorize RB. After a certain mixing time (t), aliquot samples were withdrawn and the residual persulfate was quenched by methanol. The remaining concentration of RB (C_t) was analyzed using a UV-Vis spectrophotometer at 554 nm (e-ChromTech CT-2000, Taiwan) to determine the remaining RB concentration. To investigate effects of persulfate dosage and MIL-88A loading, persulfate concentration was increased from 50 to 400 mg L^{-1}, whereas MIL-88A loading was changed from 100 to 1500 mg L^{-1}. The effect of temperature was examined by testing the RB decolorization at 20, 30, 40 and 50 °C. Effects of pH, UV irradiation and ultrasonication on the RB decolorization were also studied. The pH of RB solutions was varied from 3 to 11 by adding 0.1 M sulfuric acid and sodium hydroxide solutions. A 9 W UVA lamp (Philips PL-S9W, Netherland) was placed in the center of the batch reactor to assess the effect of UV irradiation. The effect of ultrasonication was evaluated by placing the batch reactor in a temperature-controllable ultrasonication batch (Yeong-Hsin LEO-1002S, Taiwan). Additionally, several inhibitors, including ascorbic acid, methanol and TBA were also used to examine the effects of inhibitors and to provide insight into the potential mechanism of persulfate activation by MIL-88A. All RB decolorization experiments were duplicated and repeated at least twice.

2.5 Recyclability of MIL-88A for the RB decolorization

In this study, the recyclability of MIL-88A as the catalyst to activate persulfate was also evaluated. The spent MIL-88A was collected *via* centrifugation and used without any regeneration treatment. The recovered MIL-88A was then use to decolorize in the presence of persulfate in the same manner as the pristine MIL-88A.

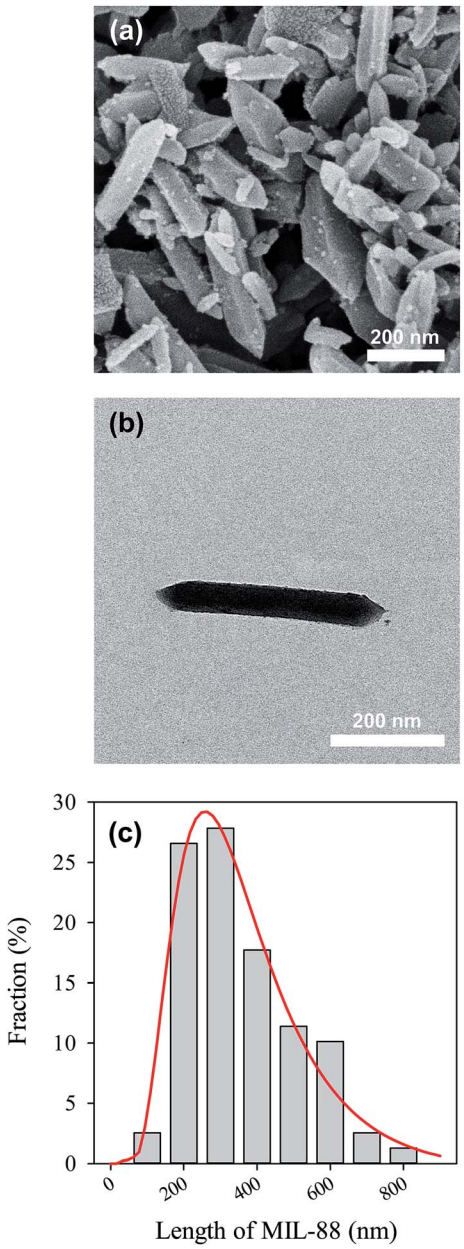

Fig. 2 Morphology of MIL-88A: (a) SEM and (b) TEM images of the as-synthesis, and (c) size (length) distribution of MIL-88A nano-rods.

3. Results and discussion

3.1 Characterization of the as-synthesized MIL-88A

The as-synthesized MIL-88A can be seen in Fig. 2(a), in which MIL-88A particles are closely-packed after the drying process. The MIL-88A particles exhibit hexagonal rod-like morphology; this is the typical shape of MIL-88A.[50,53] Although MIL-88A rods are aggregated in Fig. 2(a), these MIL-88A rods can be mono-dispersed after sonication and dispersion in solvents as seen in the TEM image (Fig. 2(b)). Fig. 2(a) and (b) also reveal that sizes (*i.e.*, lengths) of MIL-88A rods are nanometer-scale, with the size ranging from 100 to 800 nm (Fig. 2(c)). To obtain an average range, the size distribution is fitted using the log normal distribution model. The average size is 257 ± 9 nm. The crystalline structure of MIL-88A was further analyzed and shown in Fig. 3(a). It has been suggested that synthesis parameters, such as temperature, pressure, solvent selection and pH, can significantly affect the PXRD pattern and crystallinity.[53,54] Since MIL-88A in this study was synthesized in water at 85 °C under ambient pressure, the PXRD pattern agrees with the reported PXRD pattern of MIL-88A which was synthesized under similar conditions.[53] We also evaluated the IR spectrum of MIL-88A as shown in Fig. 3(b). Since MIL-88A is synthesized using fumaric acid, a number of significant bands are derived from fumaric acid. The bands at 1396 and 1603 cm^{-1} are from the symmetric and asymmetric vibration modes of the carboxyl group, respectively.[55] The band at 648 cm^{-1} is attributed to the carbonyl group.[56] Although

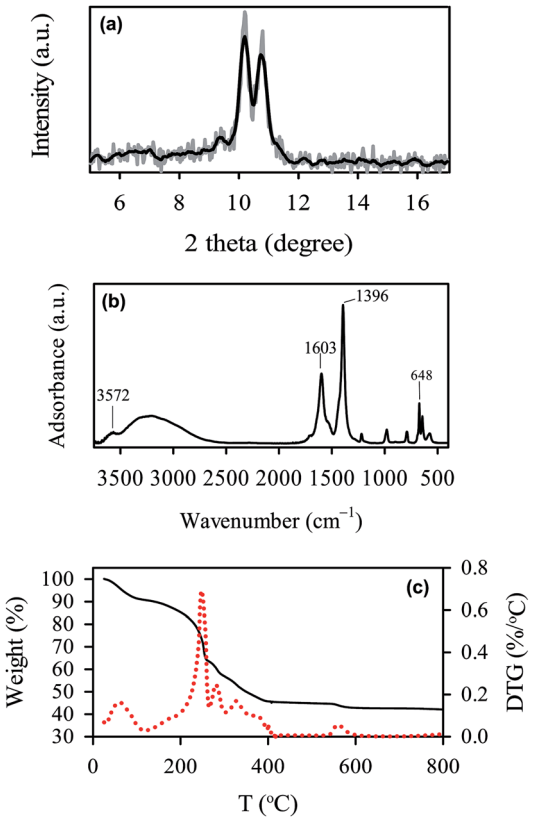

Fig. 3 Characteristics of MIL-88A: (a) XRD pattern, (b) FT-IR spectrum, and (c) TG and derivative (DTG) curves.

MIL-88A was dried in the oven to remove the synthesis solvent (*i.e.*, water), the IR spectrum of MIL-88A still exhibits a broad band in the region between 3200–3400 cm^{-1} owing to the presence of water and a short band at 3572 cm^{-1}, ascribed to the vibrational mode of OH^-. The water content might be from the adsorption of moisture in air to MIL-88A. The moisture content in MIL-88A is also revealed by the TG analysis. Fig. 3(c) shows the TG curve of MIL-88A and the corresponding derivative TG as the inset. A minor weight loss occurred below 100 °C, which could be attributed to the moisture and other gas molecules adsorbed to MIL-88A. However, the weight of MIL-88A remains quite stable up to 200 °C, when the ligand (*i.e.*, fumaric acid) starts decomposing through 400 °C.[57] Subsequently, the weight of MIL-88A is almost unchanged through 800 °C.

The chemical composition of MIL-88A was identified *via* the XPS analysis. Fig. 4 shows full survey of MIL-88A. Several significant peaks are readily recognized at binding energies of 284.4, 531.2, 711.4 and 725.2 eV, corresponding to C 1s, O 1s, Fe 2p3, and Fe 2p1, respectively. The inset of Fig. 4 also shows the Fe 2p core level of MIL-88A, in which Fe 2p1, Fe 2p2 and Fe 2p3 peaked can be clearly revealed. The peak separation between Fe 2p1 and Fe 2p3 is also determined and found to be 13.8 eV, which is comparable to the value reported for Fe_2O_3. This indicates that iron existing within MIL-88A coordinated with oxygen of fumaric acid to form iron oxide clusters in the form of Fe_2O_3.[50,58]

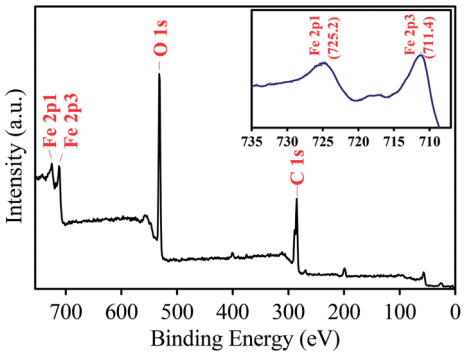

Fig. 4 XPS spectrum of full survey of the as-synthesized MIL-88A and the inset is Fe 2p core levels of MIL-88A.

3.2 Decolorization of RB using persulfate activated by MIL-88A

Prior to testing the RB decolorization using persulfate activated by MIL-88A, it was critical to examine whether the RB decolorization occurs simply *via* the adsorption to MIL-88A. To this end, MIL-88A was added to the RB solution in the absence of persulfate and the result is shown in Fig. 5. Even though MIL-88A was mixed with the RB solution for 2 hours, no noticeable amount of RB was decolorized, indicating that RB could not be removed by MIL-88A simply through the adsorption mechanism. In addition, we also evaluated the RB decolorization efficiency using persulfate alone. Fig. 5 indicates that although persulfate alone can decolorize RB, the decolorization efficiency (*i.e.*, $(C_0 - C_t)/(C_0)\%$) is quite limited (less than 20%). When MIL-88A is combined with persulfate, the RB solution is decolorized significantly; after 2 hours, the decolorization efficiency reached ~80%, showing that the combination of persulfate and MIL-88A effectively decolorized the RB solution. Since MIL-88A was unable to adsorb RB and persulfate did not decolorize RB, this result suggests that persulfate was activated in the presence of MIL-88A and in turn generated sulfate radicals to degrade RB.

Although Du *et al.* also combined a Fe-based MOF, MIL-53, with ammonium persulfate, their study was performed under

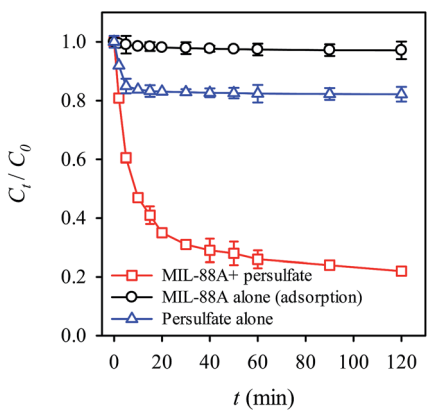

Fig. 5 RB removal by adsorption to MIL-88A, oxidation with persulfate and oxidation with persulfate activated by MIL-88A (persulfate = 200 mg L^{-1}, MIL-88A = 500 mg L^{-1}, 40 °C).

UV and visible light irradiation to generate electrons which may induce the activation of persulfate. In this study, no light (*i.e.*, UV and visible light) was permitted to photocatalytically activate persulfate to degrade dyes, even though MIL-88A and MIL-53 are both Fe^{3+}-based MOFs. Thus, there should be another pathway to activate persulfate using active sites within MIL-88A.[44] As demonstrated above, the iron oxide present within MIL-88A was found to be Fe_2O_3,[50] in which Fe is trivalent (*i.e.*, Fe^{3+}). Recently, Liu *et al.* has indicated that the presence of Fe^{3+} can initiate the decomposition of persulfate *via* one-electron reduction of Fe^{3+} as follows (eqn (1) and (2)):[59]

$$Fe^{3+} + S_2O_8^{2-} \rightarrow Fe^{2+} + S_2O_8^{\bullet -} \quad (1)$$

$$Fe^{2+} + S_2O_8^{2-} \rightarrow Fe^{3+} + SO_4^{\bullet -} + SO_4^{2-} \quad (2)$$

The appearance of $S_2O_8^{\bullet -}$ from the one-electron reduction of $S_2O_8^{2-}$ is also supported by a number of previous studies that investigated the reaction between $S_2O_8^{2-}$ and $SO_4^{\bullet -}$.[60,61] According to eqn (1) and (2), the proposed net reaction between Fe^{3+}@MIL-88A and persulfate anion ($S_2O_8^{2-}$) is summarized and illustrated in Fig. 6. In the proposed reaction, Fe^{3+}@MIL-88A reacts with persulfate ($S_2O_8^{2-}$) to generate persulfate radicals ($S_2O_8^{\bullet -}$) as Fe^{3+}@MIL-88A is reduced to Fe^{2+}@MIL-88A. At the moment Fe^{2+} persulfate MIL-88A appears, it can react with persulfate to generate sulfate radicals ($SO_4^{\bullet -}$) and Fe^{2+}@MIL-88A returns to its original state, Fe^{3+}@MIL-88A. A similar mechanism is also reported for persulfate activation using Fe^{3+} coordinated with ethylenediaminetetraacetic acid (EDTA). Liang *et al.* found that Fe^{3+} chelated with EDTA was able to activate persulfate for the degradation of trichloroethylene because Fe^{3+} was first reduced to Fe^{2+} which then activated persulfate to generate sulfate radicals.[62] EDTA was also found to play an important role considering that EDTA could simultaneously complex with Fe^{3+} and Fe^{2+}. Like EDTA, fumaric acid within MIL-88A is also composed of carboxylic acids that are coordinated with Fe^{3+}. Thus, it is believed that fumaric acid also plays a critical role in the transition between Fe^{3+} and Fe^{2+} during the activation of persulfate.

Since other MIL-88 MOFs also consist of similar iron-oxide clusters derived from the iron–carboxylate coordination, we also evaluated whether other MIL-88 MOFs could activate persulfate to decolorize RB. Considering that MIL-88B is much more structurally similar to MIL-88A, MIL-88B was selected and examined. When MIL-88B (Fig. S1(a), see ESI†) was added to a RB solution in the presence of persulfate, most of RB in water was decolorized (Fig. S1(b)†). However, we found that RB removal *via* the adsorption to MIL-88B was quite significant (*i.e.*, 80% of C_0). While almost no RB was adsorbed to MIL-88A, this high RB adsorption to MIL-88B could be owing to the benzene ring of terephthalic acid in MIL-88B, which can interact with RB *via* the π–π stacking effect.[25,63,64] This high adsorption capacity for RB can be also expected in MIL-88C and MIL-88D, which both contain two benzene rings. In order to ensure that MIL-88B did activate persulfate, as the RB decolorization test using MIL-88B and persulfate reached equilibrium, 10 mg L^{-1} of RB was again added to the mixture. The result showed that RB was still considerably decolorized (C_t/C_0 = 0.15 at equilibrium), validating MIL-88B's catalytic capability to activate persulfate.

Furthermore, the XPS spectrum of MIL-88A recovered from the reaction of persulfate activation was also analyzed and shown in Fig. S2 (see ESI†). It can be seen that the spent MIL-88A exhibits an almost identical spectrum to that of the pristine MIL-88A, showing that the chemical composition of MIL-88A remained the same even after the persulfate activation reaction. Fig. 7 also shows the detailed Fe 2p core level of the spent MIL-88A, which is the same as the pristine MIL-88A. This suggests that the iron oxide within MIL-88A still appears to be Fe_2O_3 and the state of the iron ion remained as Fe^{3+} after participating in the reactions listed in eqn (1) and (2).

3.3 Effects of persulfate dosage and MIL-88A loading on decolorization of RB

Since the persulfate dosage and MIL-88A loading are two important parameters in this persulfate activation reaction, we further investigated the effects of these factors on the RB

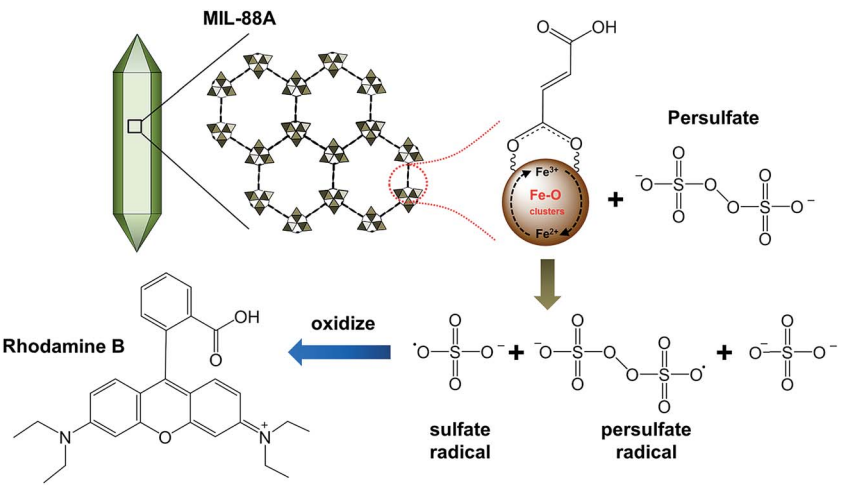

Fig. 6 A proposed mechanism for the activation of persulfate using MIL-88A.

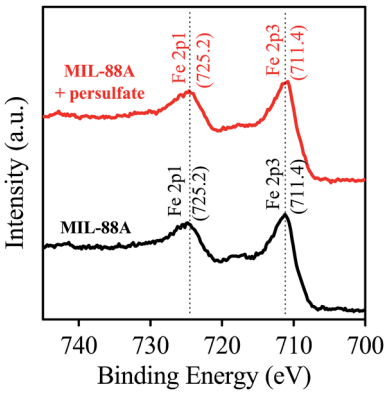

Fig. 7 XPS spectra of Fe 2p core levels of the pristine MIL-88A and MIL-88A recovered from the reaction of persulfate activation.

decolorization and attempted to obtain an optimal condition for the RB decolorization. Fig. 8 shows the decolorization efficiency of various persulfate dosages ranging from 50 to 400 mg L^{-1} and MIL-88A loadings ranging from 100 to 1500 mg L^{-1}. When the MIL-88A loading was fixed to a relatively low loading (*e.g.*, 100 or 200 mg L^{-1}), an increase in the persulfate dosage did not result in significant enhancement in the RB decolorization. Nevertheless, when the concentration of MIL-88A was fixed to 500 mg L^{-1} and greater, the increase in persulfate was found to improve the RB decolorization. This suggests that at low MIL-88A loading, the amount of MIL-88A was not sufficient to activate the existing persulfate, even though more persulfate was added to the reaction. This might be limited by mass transfer barriers. Conversely, at the high MIL-88A loading, a higher amount of persulfate was activated, leading to the improved RB decolorization. On the other hand, when the persulfate dosage was fixed and the MIL-88A loading was varied, RB decolorization changed correspondingly, regardless of the persulfate dosage. This result indicates that the MIL-88A loading was a more dominant factor in this persulfate activation reaction. Fig. 8 also reveals that when the MIL-88A loading was 1500 mg L^{-1}, the RB decolorization efficiencies at the persulfate dosages of 300 and 400 mg L^{-1} both reached nearly 100%. Therefore, to decolorize 10 mg L^{-1} of RB in water, the optimal persulfate dosage and MIL-88A loading are 300 mg L^{-1} and 1500 mg L^{-1}, respectively.

3.4 Effects of temperature and pH on the decolorization of RB

Temperature also represents an important parameter affecting the persulfate activation. Therefore, in this study, temperatures of 20, 30, 40 and 50 °C were selected to examine the effect of temperature on the persulfate activation. The corresponding RB decolorization efficiencies are displayed in Fig. 9. As the temperature increased from 20 to 30 °C, the decolorization efficiency increased notably from 35 to 55%, showing that RB decolorization is enhanced at higher temperatures. The decolorization efficiency became 75% and 95%, respectively, when the temperature was raised to 40 and 50 °C, respectively, showing the critical role of temperature in the persulfate activation and the RB decolorization. To further investigate the effect of temperature, the decolorization kinetics at each temperature was also analyzed and compared. The pseudo first order rate law has been adopted as a common kinetic model to analyze degradation reactions using persulfate. It is typically expressed as follows (eqn (3)):

$$C_t = C_0 \exp(-kt) \quad (3)$$

where k is the apparent first order rate constant of RB decolorization. The k value at each temperature is determined and listed in Table 1. The k value is found to increase as the temperature increases; the k value at 50 °C (*i.e.*, 0.220 min^{-1}) appears to be 3.5 times the k value at 20 °C (0.064 min^{-1}). This result suggests that the higher temperature not only improved the RB decolorization efficiency but also increased the decolorization kinetics.

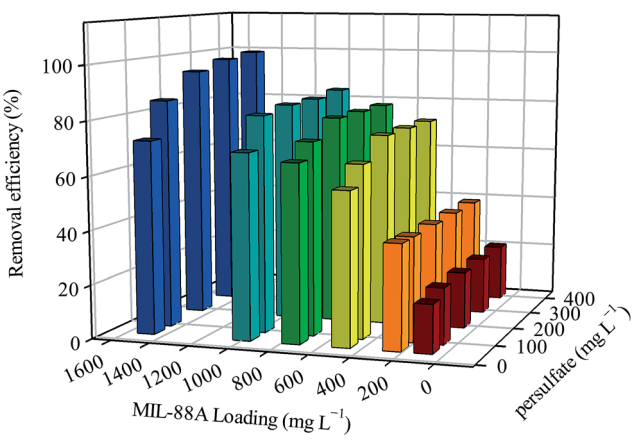

Fig. 8 Effects of persulfate dosage and MIL-88A loading on the degradation of RB using persulfate activated by MIL-88A activated oxidation (40 °C).

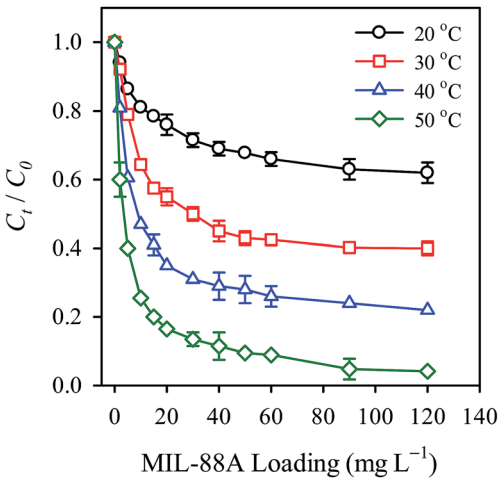

Fig. 9 Effect of temperature on the RB decolorization using persulfate activated by MIL-88A (persulfate = 200 mg L^{-1}, MIL-88A = 500 mg L^{-1}).

The relationship between k value and temperature can be correlated using the Arrhenius equation to determine the activation energy as follows (eqn (4)):

$$\ln k = \ln k_0 - \frac{E_a}{R}\frac{1}{T} \quad (4)$$

where E_a is the activation energy (kJ mol^{-1}); k_0 represents the temperature-independent factor (g mg^{-1} min^{-1}); T is the solution temperature in Kelvin (K) and R denotes the universal gas constant. According to eqn (4), a plot of ln k *versus* T^{-1} is shown in Fig. S3 (see ESI†) and the data points are well fitted using the linear regression with $R^2 = 0.977$, suggesting that the relationship between the k value and temperature can be adequately expressed by the Arrhenius equation. E_a can be also determined using eqn (4) and it was found to be 32.5 kJ mol^{-1}.

Since the solution pH is also considered as a critical factor in the persulfate activation reaction, we also examined its effect as shown in Fig. 10. As the pH was increased from 3 to 11, the removal efficiency decreased accordingly, implying that the alkaline condition are not favorable for RB decolorization using persulfate. This could be due to the self-decomposition of persulfate under basic conditions, leading to the lower decolorization efficiency.[40,65,66] In contrast, the decolorization efficiency remained quite stable in the pH range of 4–7 and even increased slightly at pH = 3. This is because the stability of persulfate is relatively high at low pH[40] and consequently the decolorization efficiency is improved.

3.5 Effects of UV, ultrasonication and inhibitors on the decolorization of RB in water

Because that the activation of persulfate can be facilitated by UV and ultrasonication irradiation,[40–42,67] we also investigated the effects of these two facilitations on the RB decolorization. Fig. 11 reveals the RB decolorization with and without the UV and ultrasonication. When the UV irradiation was introduced, the decolorization efficiency greatly enhanced. To ensure that the improvement was not due to the decomposition of RB by UV irradiation, we also examined the RB decolorization using UV irradiation alone (Fig. S4, see ESI†). Nonetheless, UV irradiation was unable to decompose RB within the testing time. Thus, the improvement might be attributed to the UV irradiation which facilitated the generation of radicals including sulfate as well as OH radicals.[41,42,67] Another possibility might be that the photocatalytic properties of MIL-88A aid decolorization efficiency.[50]

Table 1 The pseudo first order rate constant (k) of the RB decolorization (C_0 = 10 mg L^{-1}) under different conditions using persulfate activated by MIL-88A

Persulfate (mg L^{-1})	MIL-88A (mg L^{-1})	T (°C)	k (min^{-1})	R^2
200	500	20	0.064	0.973
200	500	30	0.084	0.992
200	500	40	0.131	0.980
200	500	50	0.220	0.986
200 + UV irradiation	500	40	0.461	0.950
200 + Ultrasonication	500	40	0.735	0.961

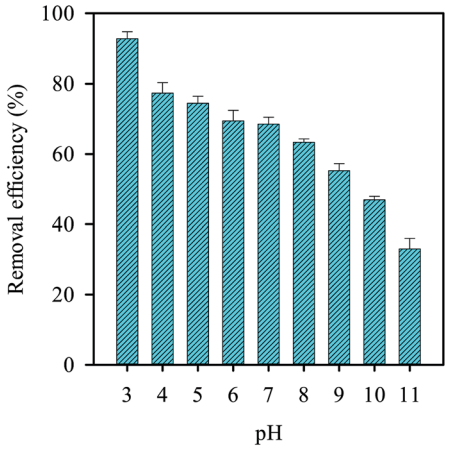

Fig. 10 Effect of pH on the RB decolorization using persulfate activated by MIL-88A (persulfate = 200 mg L^{-1}, MIL-88A = 500 mg L^{-1}, 40 °C).

The UV irradiation of MIL-88A could generate electrons that induce the decomposition of persulfate, thereby generating sulfate radicals. Furthermore, the decolorization kinetics was also determined (Table 1) and the k value was found to be 2.5 times higher than the k value observed without the UV irradiation. Additionally, Fig. 11 shows the RB decolorization with ultrasonication. One can see that the RB decolorization efficiency is even greater with ultrasonication. The kinetics with ultrasonication was also found to increase considerably, indicating that ultrasonication appears to facilitate to the activation of persulfate. This could be because the energy derived from the ultrasonication promotes the generation of free radicals and thus enhances the RB decolorization.[40]

We also examined the effects of various inhibitors on the activation of persulfate and RB decolorization, providing additional insights into the mechanism of decolorization using persulfate activated by MIL-88A. We first examined the effect of ascorbic acid, a typical radical scavenger, on the RB

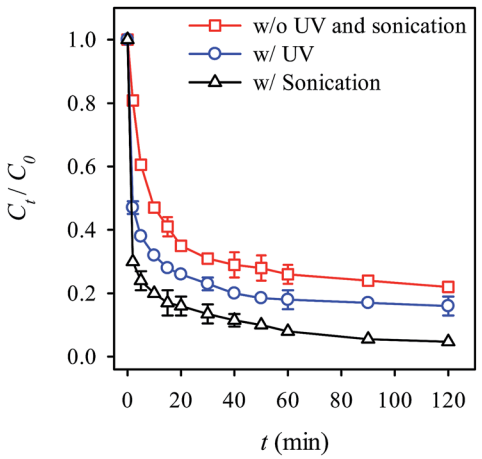

Fig. 11 Effects of UV and ultrasonication on the RB decolorization using persulfate activated by MIL-88A (persulfate = 200 mg L^{-1}, MIL-88A = 500 mg L^{-1}, 40 °C).

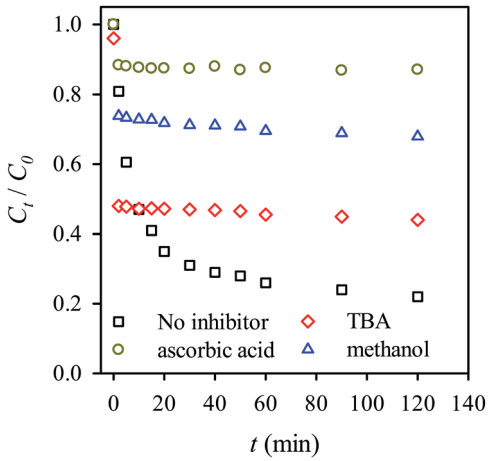

Fig. 12 Effects of inhibitors on the RB decolorization using persulfate activated by MIL-88A (persulfate = 200 mg L^{-1}, MIL-88A = 500 mg L^{-1}, 40 °C, ascorbic acid = 280 mmol L^{-1}, *tert*-butyl alcohol (TBA) = 280 mmol L^{-1}, methanol = 280 mmol L^{-1}).

decolorization (Fig. 12). Only 12% of RB is decolorized when ascorbic acid is present in the persulfate-MIL-88A system. Compared to the RB decolorization in the absence of scavengers, the decolorization efficiency was much lower, indicating that the presence of ascorbic acid tremendously scavenged radicals and inhibited the decolorization. This also reveals the important role of radicals in the RB decolorization. Typically, the activation of persulfate generates sulfate radicals which may also induce the generation of hydroxyl radicals. Thus, to further determine contribution of each radical species, methanol, a universal radical scavenger, and TBA, a specific hydroxyl-radical scavenger, were used to investigate inhibiting effects in Fig. 12. When TBA was present in the persulfate-MIL-88A system, the RB decolorization efficiency became 44%, whereas the decolorization efficiency was 68% in the presence of methanol. This result suggests that both the sulfate and hydroxyl radicals contributed to the RB decolorization, although the hydroxyl radical played a lesser role.

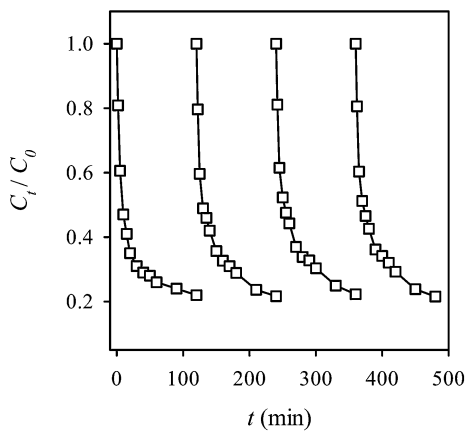

Fig. 13 Recyclability of MIL-88A to activate persulfate for the RB decolorization (persulfate = 200 mg L^{-1}, MIL-88A = 500 mg L^{-1}, 40 °C).

3.6 Recyclability of MIL-88A for the activation of persulfate

Recyclability represents one of the most important properties of a heterogeneous catalyst. Thus, the recyclability of MIL-88A was evaluated by using MIL-88A to activate for multiple cycles without additional treatment on the spent MIL-88A. Fig. 13 shows 4 cycles of the RB decolorization using the persulfate-MIL-88A system. It can be seen that even after 4 cycles, MIL-88A still exhibited a stable and effective catalytic activity to activate persulfate and to decolorize RB, and no noticeable activity loss was observed. This result indicates that MIL-88A can be re-used to activate persulfate without additional regeneration of spent MIL-88A.

4. Conclusion

This study marks the first attempt to use MIL-88A, a DMF-free, iron-based MOF, as a heterogeneous catalyst to activate persulfate for the decolorization of RB dye in water. Through the coordination of Fe^{3+} and fumaric acid, iron oxide cluster (*i.e.*, Fe_2O_3) forms within MIL-88A. Fe^{3+} of Fe_2O_3 induced the generation of persulfate radicals which in turn lead to the formation of sulfate radicals to decolorize RB dye. Factors influencing the activation of persulfate and RB decolorization were examined including persulfate dosage, MIL-88A loading, temperature, pH, UV and US irradiation as well as inhibitors. MIL-88A was also found to be used for the multiple-cycle activation of persulfate without additional regeneration of the spent MIL-88A. These features make MIL-88A an effective and recyclable heterogeneous catalyst for the activation of persulfate. Most importantly, unlike other iron-containing MOFs, MIL-88A can be synthesized just in water without using toxic solvents such as DMF.

Acknowledgements

The authors thank Mr Andrew P. Jochems at New Mexico Bureau of Geology & Mineral Resources for his suggestions on the English writing.

References

1 N. Stock and S. Biswas, Synthesis of Metal–Organic Frameworks (MOFs): Routes to Various MOF Topologies, Morphologies, and Composites, *Chem. Rev.*, 2011, **112**, 933–969.
2 C. Janiak and J. K. Vieth, MOFs, MILs and more: concepts, properties and applications for porous coordination networks (PCNs), *New J. Chem.*, 2010, **34**, 2366–2388.
3 U. Mueller, M. Schubert, F. Teich, H. Puetter, K. Schierle-Arndt and J. Pastre, Metal–organic frameworks-prospective industrial applications, *J. Mater. Chem.*, 2006, **16**, 626–636.
4 N. L. Rosi, J. Eckert, M. Eddaoudi, D. T. Vodak, J. Kim, M. O'Keeffe and O. M. Yaghi, Hydrogen Storage in Microporous Metal–Organic Frameworks, *Science*, 2003, **300**, 1127–1129.

5 J. W. Yoon, S. H. Jhung, Y. K. Hwang, S. M. Humphrey, P. T. Wood and J. S. Chang, Gas-Sorption Selectivity of CUK-1: A Porous Coordination Solid Made of Cobalt(II) and Pyridine-2,4-Dicarboxylic Acid, *Adv. Mater.*, 2007, **19**, 1830–1834.

6 J.-R. Li, Y. Ma, M. C. McCarthy, J. Sculley, J. Yu, H.-K. Jeong, P. B. Balbuena and H.-C. Zhou, Carbon dioxide capture-related gas adsorption and separation in metal–organic frameworks, *Coord. Chem. Rev.*, 2011, **255**, 1791–1823.

7 J.-R. Li, R. J. Kuppler and H.-C. Zhou, Selective gas adsorption and separation in metal–organic frameworks, *Chem. Soc. Rev.*, 2009, **38**, 1477–1504.

8 J. Lee, O. K. Farha, J. Roberts, K. A. Scheidt, S. T. Nguyen and J. T. Hupp, Metal–organic framework materials as catalysts, *Chem. Soc. Rev.*, 2009, **38**, 1450–1459.

9 A. Corma, H. García and F. X. Llabrés i Xamena, Engineering Metal Organic Frameworks for Heterogeneous Catalysis, *Chem. Rev.*, 2010, **110**, 4606–4655.

10 J. Gascon, A. Corma, F. Kapteijn and F. X. Llabrés i Xamena, Metal Organic Framework Catalysis: Quo vadis?, *ACS Catal.*, 2013, 361–378.

11 P. Horcajada, T. Chalati, C. Serre, B. Gillet, C. Sebrie, T. Baati, J. F. Eubank, D. Heurtaux, P. Clayette, C. Kreuz, J.-S. Chang, Y. K. Hwang, V. Marsaud, P.-N. Bories, L. Cynober, S. Gil, G. Ferey, P. Couvreur and R. Gref, Porous metal–organic-framework nanoscale carriers as a potential platform for drug delivery and imaging, *Nat. Mater.*, 2010, **9**, 172–178.

12 Y. Cui, Y. Yue, G. Qian and B. Chen, Luminescent Functional Metal–Organic Frameworks, *Chem. Rev.*, 2011, **112**, 1126–1162.

13 L.-G. Qiu, Z.-Q. Li, Y. Wu, W. Wang, T. Xu and X. Jiang, Facile synthesis of nanocrystals of a microporous metal–organic framework by an ultrasonic method and selective sensing of organoamines, *Chem. Commun.*, 2008, 3642–3644.

14 K. S. Park, Z. Ni, A. P. Côté, J. Y. Choi, R. Huang, F. J. Uribe-Romo, H. K. Chae, M. O'Keeffe and O. M. Yaghi, Exceptional chemical and thermal stability of zeolitic imidazolate frameworks, *Proc. Natl. Acad. Sci. U. S. A.*, 2006, **103**, 10186–10191.

15 R. Ahmad, A. G. Wong-Foy and A. J. Matzger, Microporous Coordination Polymers As Selective Sorbents for Liquid Chromatography, *Langmuir*, 2009, **25**, 11977–11979.

16 S. El-Hankari, J. Huo, A. Ahmed, H. Zhang and D. Bradshaw, Surface etching of HKUST-1 promoted *via* supramolecular interactions for chromatography, *J. Mater. Chem. A*, 2014, **2**, 13479–13485.

17 A. Ahmed, M. Forster, R. Clowes, D. Bradshaw, P. Myers and H. Zhang, Silica SOS@HKUST-1 composite microspheres as easily packed stationary phases for fast separation, *J. Mater. Chem. A*, 2013, **1**, 3276–3286.

18 N. A. Khan, Z. Hasan and S. H. Jhung, Adsorptive removal of hazardous materials using metal–organic frameworks (MOFs): a review, *J. Hazard. Mater.*, 2013, **244–245**, 444–456.

19 Z. Hasan and S. H. Jhung, Removal of hazardous organics from water using metal–organic frameworks (MOFs): plausible mechanisms for selective adsorptions, *J. Hazard. Mater.*, 2015, **283**, 329–339.

20 M. Zhao, S. Ou and C.-D. Wu, Porous Metal–Organic Frameworks for Heterogeneous Biomimetic Catalysis, *Acc. Chem. Res.*, 2014, **47**, 1199–1207.

21 M. Ranocchiari and J. A. v. Bokhoven, Catalysis by metal–organic frameworks: fundamentals and opportunities, *Phys. Chem. Chem. Phys.*, 2011, **13**, 6388–6396.

22 X. Zhao, D. Liu, H. Huang, W. Zhang, Q. Yang and C. Zhong, The stability and defluoridation performance of MOFs in fluoride solutions, *Microporous Mesoporous Mater.*, 2014, **185**, 72–78.

23 F. Ke, L.-G. Qiu, Y.-P. Yuan, F.-M. Peng, X. Jiang, A.-J. Xie, Y.-H. Shen and J.-F. Zhu, Thiol-functionalization of metal–organic framework by a facile coordination-based postsynthetic strategy and enhanced removal of Hg^{2+} from water, *J. Hazard. Mater.*, 2011, **196**, 36–43.

24 L. Li, J. C. Li, Z. Rao, G. W. Song and B. Hu, Metal Organic Framework $[Cu_3(BTC)_2(H_2O)_3]$ for the adsorption of methylene blue from aqueous solution, *Desalin. Water Treat.*, 2013, 1–7.

25 B. K. Jung, Z. Hasan and S. H. Jhung, Adsorptive removal of 2,4-dichlorophenoxyacetic acid (2,4-D) from water with a metal–organic framework, *Chem. Eng. J.*, 2013, **234**, 99–105.

26 K.-Y. A. Lin, H. Yang, C. Petit and F.-K. Hsu, Removing oil droplets from water using a copper-based metal organic frameworks, *Chem. Eng. J.*, 2014, **249**, 293–301.

27 K.-Y. A. Lin and Y.-T. Hsieh, Copper-based Metal Organic Framework (MOF), HKUST-1, as an Efficient Adsorbent to Remove *p*-Nitrophenol from Water, *J. Taiwan Inst. Chem. Eng.*, 2015, DOI: 10.1016/j.jtice.2014.12.008, in press.

28 J.-Q. Jiang, C.-X. Yang and X.-P. Yan, Zeolitic Imidazolate Framework-8 for Fast Adsorption and Removal of Benzotriazoles from Aqueous Solution, *ACS Appl. Mater. Interfaces*, 2013, **5**, 9837–9842.

29 K.-Y. A. Lin and H.-A. Chang, Efficient Adsorptive Removal of Humic Acid from Water using Zeolitic Imidazole Framework-8 (ZIF-8), *Water, Air, Soil Pollut.*, 2015, **226**(10), DOI: 10.1007/s11270-014-2280-7.

30 P. Mahata, G. Madras and S. Natarajan, New photocatalysts based on mixed-metal pyridine dicarboxylates, *Catal. Lett.*, 2007, **115**, 27–32.

31 Y. Fu, D. Sun, Y. Chen, R. Huang, Z. Ding, X. Fu and Z. Li, An Amine-Functionalized Titanium Metal–Organic Framework Photocatalyst with Visible-Light-Induced Activity for CO_2 Reduction, *Angew. Chem., Int. Ed.*, 2012, **51**, 3364–3367.

32 C.-F. Zhang, L.-G. Qiu, F. Ke, Y.-J. Zhu, Y.-P. Yuan, G.-S. Xu and X. Jiang, A novel magnetic recyclable photocatalyst based on a core–shell metal–organic framework Fe_3O_4@MIL-100(Fe) for the decolorization of methylene blue dye, *J. Mater. Chem. A*, 2013, **1**, 14329–14334.

33 C. G. Silva, A. Corma and H. Garcia, Metal–organic frameworks as semiconductors, *J. Mater. Chem.*, 2010, **20**, 3141–3156.

34 M. Alvaro, E. Carbonell, B. Ferrer, F. X. Llabrés i Xamena and H. Garcia, Semiconductor Behavior of a Metal–Organic Framework (MOF), *Chem.–Eur. J.*, 2007, **13**, 5106–5112.

35 M. Martis, W. Meicheng, K. Mori and H. Yamashita, Fabrication of metal nanoparticles in metal organic framework NH_2-MIL-125 by UV photo-assisted methods for optimized catalytic properties, *Catal. Today*, 2014, **235**, 98–102.

36 M. Wen, K. Mori, T. Kamegawa and H. Yamashita, Amine-functionalized MIL-101(Cr) with imbedded platinum nanoparticles as a durable photocatalyst for hydrogen production from water, *Chem. Commun.*, 2014, **50**, 11645–11648.

37 C. Gomes Silva, I. Luz, F. X. Llabrés i Xamena, A. Corma and H. García, Water Stable Zr–Benzenedicarboxylate Metal–Organic Frameworks as Photocatalysts for Hydrogen Generation, *Chem.–Eur. J.*, 2010, **16**, 11133–11138.

38 L. Shen, S. Liang, W. Wu, R. Liang and L. Wu, Multifunctional NH_2-mediated zirconium metal–organic framework as an efficient visible-light-driven photocatalyst for selective oxidation of alcohols and reduction of aqueous Cr(VI), *Dalton Trans.*, 2013, **42**, 13649–13657.

39 D. Sun, Y. Fu, W. Liu, L. Ye, D. Wang, L. Yang, X. Fu and Z. Li, Studies on Photocatalytic CO_2 Reduction over NH_2-Uio-66(Zr) and Its Derivatives: Towards a Better Understanding of Photocatalysis on Metal–Organic Frameworks, *Eur. J. Chem.*, 2013, **19**, 14279–14285.

40 W. Guo, S. Su, C. Yi and Z. Ma, Degradation of antibiotics amoxicillin by Co_3O_4-catalyzed peroxymonosulfate system, *Environ. Prog. Sustainable Energy*, 2013, **32**, 193–197.

41 E. R. Bandala, M. A. Peláez, D. D. Dionysiou, S. Gelover, J. Garcia and D. Macías, Degradation of 2,4-dichlorophenoxyacetic acid (2,4-D) using cobalt-peroxymonosulfate in Fenton-like process, *J. Photochem. Photobiol., A*, 2007, **186**, 357–363.

42 G. P. Anipsitakis and D. D. Dionysiou, Transition metal/UV-based advanced oxidation technologies for water decontamination, *Appl. Catal., B*, 2004, **54**, 155–163.

43 P. K. Malik and S. K. Saha, Oxidation of direct dyes with hydrogen peroxide using ferrous ion as catalyst, *Sep. Purif. Technol.*, 2003, **31**, 241–250.

44 J.-J. Du, Y.-P. Yuan, J.-X. Sun, F.-M. Peng, X. Jiang, L.-G. Qiu, A.-J. Xie, Y.-H. Shen and J.-F. Zhu, New photocatalysts based on MIL-53 metal–organic frameworks for the decolorization of methylene blue dye, *J. Hazard. Mater.*, 2011, **190**, 945–951.

45 L. Ai, C. Zhang, L. Li and J. Jiang, Iron terephthalate metal–organic framework: revealing the effective activation of hydrogen peroxide for the degradation of organic dye under visible light irradiation, *Appl. Catal., B*, 2014, **148–149**, 191–200.

46 S. Bhattacharjee, J.-S. Choi, S.-T. Yang, S. B. Choi, J. Kim and W.-S. Ahn, Solvothermal Synthesis of Fe-MOF-74 and Its Catalytic Properties in Phenol Hydroxylation, *J. Nanosci. Nanotechnol.*, 2010, **10**, 135–141.

47 T. A. Vu, G. H. Le, C. D. Dao, L. Q. Dang, K. T. Nguyen, P. T. Dang, H. T. K. Tran, Q. T. Duong, T. V. Nguyen and G. D. Lee, Isomorphous substitution of Cr by Fe in MIL-101 framework and its application as a novel heterogeneous photo-Fenton catalyst for reactive dye degradation, *RSC Adv.*, 2014, **4**, 41185–41194.

48 R. J. Kennedy and A. M. Stock, The Oxidation of Organic Substances by Potassium Peroxymonosulfate, *J. Org. Chem.*, 1960, **25**, 1901–1906.

49 S. Muhammad, E. Saputra, H. Sun, J. d. C. Izidoro, D. A. Fungaro, H. M. Ang, M. O. Tade and S. Wang, Coal fly ash supported Co_3O_4 catalysts for phenol degradation using peroxymonosulfate, *RSC Adv.*, 2012, **2**, 5645–5650.

50 W.-T. Xu, L. Ma, F. Ke, F.-M. Peng, G.-S. Xu, Y.-H. Shen, J.-F. Zhu, L.-G. Qiu and Y.-P. Yuan, Metal–organic frameworks MIL-88A hexagonal microrods as a new photocatalyst for efficient decolorization of methylene blue dye, *Dalton Trans.*, 2014, **43**, 3792–3798.

51 C. Serre, C. Mellot-Draznieks, S. Surblé, N. Audebrand, Y. Filinchuk and G. Férey, Role of Solvent–Host Interactions That Lead to Very Large Swelling of Hybrid Frameworks, *Science*, 2007, **315**, 1828–1831.

52 M. Ma, H. Noei, B. Mienert, J. Niesel, E. Bill, M. Muhler, R. A. Fischer, Y. Wang, U. Schatzschneider and N. Metzler-Nolte, Iron Metal–Organic Frameworks MIL-88B and NH_2-MIL-88B for the Loading and Delivery of the Gasotransmitter Carbon Monoxide, *Eur. J. Chem.*, 2013, **19**, 6785–6790.

53 T. Chalati, P. Horcajada, R. Gref, P. Couvreur and C. Serre, Optimisation of the synthesis of MOF nanoparticles made of flexible porous iron fumarate MIL-88A, *J. Mater. Chem.*, 2011, **21**, 2220–2227.

54 C. Mellot-Draznieks, C. Serre, S. Surblé, N. Audebrand and G. Férey, Very Large Swelling in Hybrid Frameworks: A Combined Computational and Powder Diffraction Study, *J. Am. Chem. Soc.*, 2005, **127**, 16273–16278.

55 J. J. Najera, C. J. Percival and A. B. Horn, Infrared spectroscopic studies of the heterogeneous reaction of ozone with dry maleic and fumaric acid aerosol particles, *Phys. Chem. Chem. Phys.*, 2009, **11**, 9093–9103.

56 E. M. S. Maçôas, R. Fausto, J. Lundell, M. Pettersson, L. Khriachtchev and M. Räsänen, A Matrix Isolation Spectroscopic and Quantum Chemical Study of Fumaric and Maleic Acid, *J. Phys. Chem. A*, 2001, **105**, 3922–3933.

57 E. Y. Ionashiro, F. J. Caires, A. B. Siqueira, L. S. Lima and C. T. Carvalho, Thermal behaviour of fumaric acid, sodium fumarate and its compounds with light trivalent lanthanides in air atmosphere, *J. Therm. Anal. Calorim.*, 2012, **108**, 1183–1188.

58 H. Bao, X. Chen, J. Fang, Z. Jiang and W. Huang, Structure–Activity Relation of Fe_2O_3–CeO_2 Composite Catalysts in CO Oxidation, *Catal. Lett.*, 2008, **125**, 160–167.

59 H. Liu, T. A. Bruton, F. M. Doyle and D. L. Sedlak, *In Situ* Chemical Oxidation of Contaminated Groundwater by Persulfate: Decomposition by Fe(III)- and Mn(IV)-Containing Oxides and Aquifer Materials, *Environ. Sci. Technol.*, 2014, **48**, 10330–10336.

60 W. J. McElroy and S. J. Waygood, Kinetics of the reactions of the SO radical with SO, S_2O, H_2O and Fe^{2+}, *J. Chem. Soc., Faraday Trans.*, 1990, **86**, 2557–2564

61 X.-Y. Yu, Z.-C. Bao and J. R. Barker, Free Radical Reactions Involving $Cl^{\bullet}$, $Cl^{2-\bullet}$ and $SO_4^{-\bullet}$ in the 248 nm Photolysis of

Aqueous Solutions Containing $S_2O_8^{2-}$ and Cl, *J. Phys. Chem. A*, 2003, **108**, 295–308.

62 C. Liang, C.-P. Liang and C.-C. Chen, pH dependence of persulfate activation by EDTA/Fe(III) for degradation of trichloroethylene, *J. Contam. Hydrol.*, 2009, **106**, 173–182.

63 N. A. Khan, B. K. Jung, Z. Hasan and S. H. Jhung, Adsorption and removal of phthalic acid and diethyl phthalate from water with zeolitic imidazolate and metal–organic frameworks, *J. Hazard. Mater.*, 2015, **282**, 194–200.

64 K.-Y. A. Lin and H.-A. Chang, Ultra-high adsorption capacity of zeolitic imidazole framework-67 (ZIF-67) for removal of malachite green from water, *Chemosphere*, 2015, DOI: 10.1016/j.chemosphere.2015.01.041.

65 A. Rastogi, S. R. Al-Abed and D. D. Dionysiou, Sulfate radical-based ferrous–peroxymonosulfate oxidative system for PCBs degradation in aqueous and sediment systems, *Appl. Catal., B*, 2009, **85**, 171–179.

66 J. Sun, X. Li, J. Feng and X. Tian, Oxone/Co^{2+} oxidation as an advanced oxidation process: comparison with traditional Fenton oxidation for treatment of landfill leachate, *Water Res.*, 2009, **43**, 4363–4369.

67 J. Sun, M. Song, J. Feng and Y. Pi, Highly efficient degradation of ofloxacin by UV/Oxone/Co^{2+} oxidation process, *Environ. Sci. Pollut. Res.*, 2012, **19**, 1536–1543.